Supporting Information

Novel bio-solar hybrid photoelectrochemical synthesis for selective hydrogen peroxide production

Rusen Zou[a1], Babak Rezaei[b1], Xiaoyong Yang[c], Wenjing Zhang[a], Stephan Sylvest Keller[b], Yifeng Zhang[a]*

[a] Department of Environmental and Resource Engineering, Technical University of Denmark, DK-2800 Lyngby, Denmark

[b] National Centre for Nano Fabrication and Characterization, DTU Nanolab, Technical University of Denmark, 2800 Kgs. Lyngby, Denmark

[c] School of Environmental and Material Engineering, Yantai University, Yantai, Shandong, 264005, China

*Corresponding author:

Dr. Yifeng Zhang

Department of Environmental and Resource Engineering, Technical University of Denmark, Denmark

Tel: (+45) 45251410

Fax: (+45) 45933850

E-mail address: yifz@dtu.dk; yifzmfc@gmail.com

[1] These authors contributed equally.

Supporting Information 22 Pages, 3 Texts, 2 Tables and 12 Figures.

List of text, table and figure captions

Text. S1. Chemicals and Reagents

20 recalcitrant micropollutants are the following. **Antidepressants**: citalopram (26 μg L^{-1}) and venlafaxine (26 μg L^{-1}); **Immunosuppressant**: mycophenolic acid (30 μg L^{-1}); **Antibiotics**: azithromycin (51 μg L^{-1}); **Blood pressure regulators and lipid-lowering agent**: metoprolol (26 μg L^{-1}), hydrochlorothiazide (26 μg L^{-1}), sulfamethoxazole (130 μg L^{-1}), and bezafibrate (30 μg L^{-1}); **X-ray contrast media**: iohexol (30 μg L^{-1}) and iopromide (55 μg L^{-1}); **Analgesics**: carbamazepine (27 μg L^{-1}), diclofenac (23 μg L^{-1}) and mefenamic acid (20 μg L^{-1}); **Anti-inflammatory**: ketoprofen (80 μg L^{-1}) and bicalutamide (26 μg L^{-1}); **Anti-corrosion**: 1-H-benzotriazole (28 μg L^{-1}), 5-chlorobenzotriazole (28 μg L^{-1}) and 5- methyl-1H-benzotriazole (27 μg L^{-1}); **Herbicide**: clofibric acid (30 μg L^{-1}).

All the chemicals were used as received without further purification. All reagent solutions were prepared with ultrapure water (18.2 MΩ cm) produced from a PURELAB flex purification system (Holm & Halby, Denmark). WWTPs secondary effluent were collected from Skovshoved and Lyngby WWTP, Copenhagen, Denmark, respectively. The natural water samples were filtered by 0.45 μm cellulose acetate membrane before use, and the main water quality parameters were listed in **Table S2**.

Text. S2. Detailed calculation methods of the Faradaic efficiency

The current efficiency (CE, %) for electrosynthesis of H_2O_2 in the MES was calculated according to Eq. (1).

$$CE\ (\%) = \frac{nFVC}{Q} \times 100 \quad (1)$$

where n is the number of electrons transferred per mole H_2O_2 generated (n = 2 H_2O_2) F is Faraday's number (96,485 *10^4 C mol^{-1}), V is the catholyte volume (0.18 L), C is the molar concentration of H_2O_2 measured, and Q is the cumulative charge injected during operation (C). For the computation of Q the current in the MES is recorded and multiplied with the electrolysis time t (s).

Text. S3. Detailed operating parameters of the HPLC-MS/MS system

For analysis, 900 µL of filtered samples was transferred into a HPLC vial and 100 µL of internal standard was afterwards added into the HPLC vial. Lastly, 10 µL of sample from the HPLC vial was injected and analyzed by HPLC-MS/MS.

The HPLC system consisted of a pump, a column oven, a degasser and an auto-sampler and was from Agilent 1290 Infinity, USA. Chromatographic separation was performed using a C18 column (2.1 mm x 50 mm, 1.8 µm, Eclipse Agilent, USA). The temperature of the HPLC column oven was 35 ºC, and the constant flow rate was 0.6 mL min^{-1}. The HPLC gradient of 0.1 % formic acid in ultrapure water (solvent A) and 0.1% formic acid in acetonitrile (solvent B) was used in ESI + mode, while 5 mM ammonium formate in ultrapure water (solvent A) and 5 mM ammonium formate in 90% Actonitrile/10% ultrapure water was used in ESI-mode. The mass spectrometer equipped with the triple quadrupole was from Agilent (6470 series) USA.

Dynamic multiple reaction monitoring (MRM), which can automatically separate the transitions of micropollutants into multiple MRM tables according to the retention time window for each transition, was implemented for ESI + modes. For the analysis under ESI + mode, the HPLC gradient was initiated with 0% B for 2 min, followed by increasing the gradient B to 15 %, 20 %, 36 %, 45 %, 60 %, and 75 % after 2 min, 3 min, 2 min, 1 min, 2 min and 2 min, respectively. Before each injection, initial gradient conditions were re-established for 3 min. Nitrogen was used as the sheath gas as well as the collision gas. For the analysis under ESI- mode, a normal MRM method was implemented. The HPLC gradient was initiated with 0% B, followed by a linear increase of gradient B up to 60 % within 8 min. Initial gradient conditions were also re-established for 3 min. For both ESI + and ESI-, the sheath gas flow was 12 L min^{-1} with the temperature of 400 °C, while the gas flow was 10 L min^{-1} with the

temperature of 260 °C. The voltage for the capillary was 4500 V. The voltage for ESI + and ESI- was 500 and 0 V, respectively.

Table S1. Previous studies on (microbial) electrosynthesis of H_2O_2 using different types of cathode electrodes.

System types	Cathode materials	Operating conditions	Reactor volume	H_2O_2 production rate	Energy consumption	References
MFC	2D Graphite	pH of 7 and 100 mM Na_2SO_4 and cathodic aeration rate of 191 mL min^{-1}	160 mL (80 mL of cathode)	6.6 mg L^{-1} h^{-1}	-	[1]
MFC	Nitric acid pretreatment of 3D graphite cathode	pH of 7 and 50 mM Na_2SO_4	82 mL (50 mL of cathode)	1.5 mg L^{-1} h^{-1}	-	[2]
MFC	3D electrochemically modified graphite/carbon black/active carbon particle	pH of 7 and 50 mM Na_2SO_4	204.5 mL (120 mL of cathode)	6.8/7.1/8.1 mg L^{-1} h^{-1}	-	[3]
MEC	3D Electrochemically modified graphite particle	pH of 7, 50 mM Na_2SO_4, and applied voltage of 0.4 V	96 mL (64 mL of cathode)	88.2 mg L^{-1} h^{-1}	0.7 kWh kg^{-1} H_2O_2	[4]
MEC	2D Carbon black and graphite hybrid air cathode	pH of 7, 50 mM NaCl, cathodic aeration rate of 1500 mL min^{-1}, and applied voltage of 0.6 V	42 mL (14 mL of cathode)	3.3 mg L^{-1} h^{-1}	-	[5]
MEC	2D vulcan carbon coated GDE	pH of 7, 200 mM NaCl, cathodic aeration rate of 20 mL min^{-1}, and applied voltage of 0.31 V	218 mL (18 mL of cathode)	8.8 mg L^{-1} h^{-1}	1.1 kWh kg^{-1} H_2O_2	[6]

Table S1. (Continued)

System types	Cathode materials	Operating conditions	Reactor volume	H_2O_2 production rate	Energy consumption	References
MEC	2D GDE	pH of 7, 50 mM NaCl, and applied voltage of 0.9 V	18.8 mL (9.4 mL of cathode)	4.2 mg L^{-1} h^{-1}	1.8 kWh kg^{-1} H_2O_2	7
MEC	2D Carbon GDE	Tap water, cathodic aeration rate of 2000 mL min^{-1}, and applied voltage of 1.0-1.6 V (CEM) or 1.6-2.0 V(AEM)	110 L (10 L of cathode)	0.02 mg L^{-1} h^{-1} (AEM) and 0.28 mg L^{-1} h^{-1} (CEM)	-	8
MEC	10 of 2D Graphites	pH of 3, 50 mM Na_2SO_4, cathodic aeration rate of 400 mL min^{-1}, and applied voltage of 0.6 V	20 L (10 L of cathode)	10.82 mg L^{-1} h^{-1}	0.3 kWh kg^{-1} H_2O_2	9
MEC	Additive manufacturing-derived free-standing 3D pyrolytic carbon electrode	pH of 2, 50 mM Na_2SO_4, cathodic aeration rate of 3.6 mL min^{-1}, and applied voltage of 0.4 V	360 mL (180 mL of cathode)	10.77 mg L^{-1} h^{-1}	1.0 kWh kg^{-1} H_2O_2	10
BSPS	pTTh/GP photocathode	pH of 2, 50 mM Na_2SO_4, and cathodic aeration rate of 2 mL min^{-1}	360 mL (180 mL of cathode)	19.38 mg L^{-1} h^{-1} (applied voltage of 0.1V) and 16.29 mg L^{-1} h^{-1} (without applied voltage)	0.1 kWh kg^{-1} H_2O_2 (applied voltage of 0.1V)	In this study

Table. S2. Main characteristics of WWTP secondary effluent.

Indexes	Values
Conductivity	1319 μs cm^{-1}
pH	7.65
DO	7.53 mg L^{-1} (22.3℃)
TOC	25.48 mg L^{-1}
COD	68.77 mg L^{-1}
TS	2.82 mg L^{-1}
NO_X-N	2.25 mg L^{-1}
NH_4-N	3.42 mg L^{-1}
PO_4-P	0.59 mg L^{-1}
SO_4^{2-}	22.05 mg L^{-1}
Cl^-	230.04 mg L^{-1}

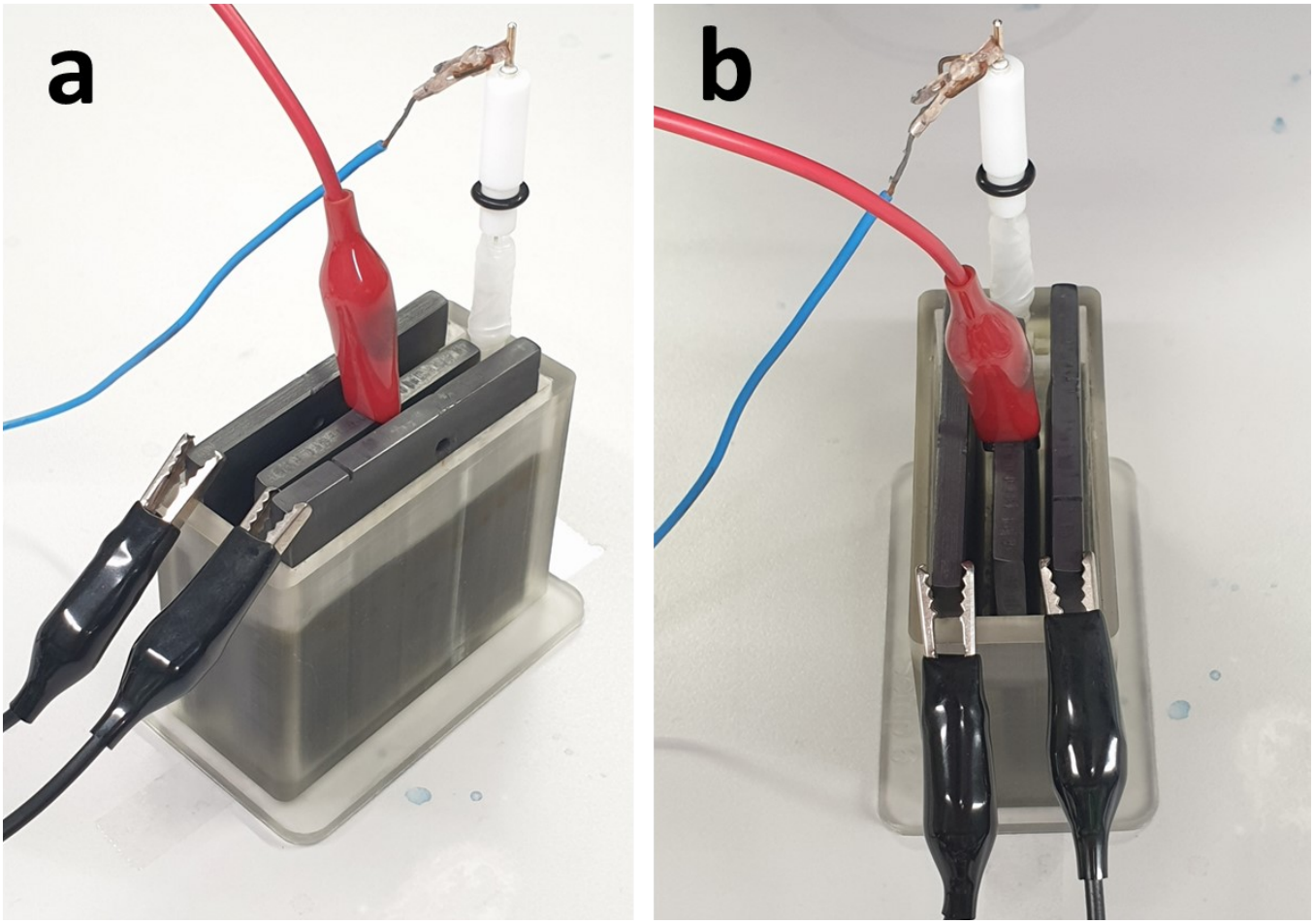

Fig. S1. Side view (a) and top view (b) of the custom-made electrochemical setup employed for electropolymerization of pTTh on the surface of GP.

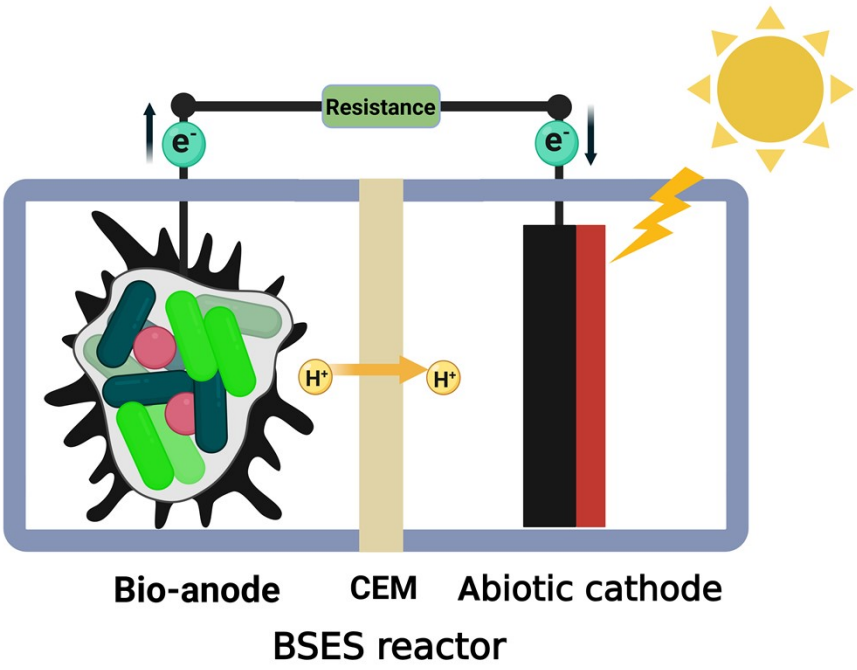

Fig. S2. Schematic representation of the BSPS reactor.

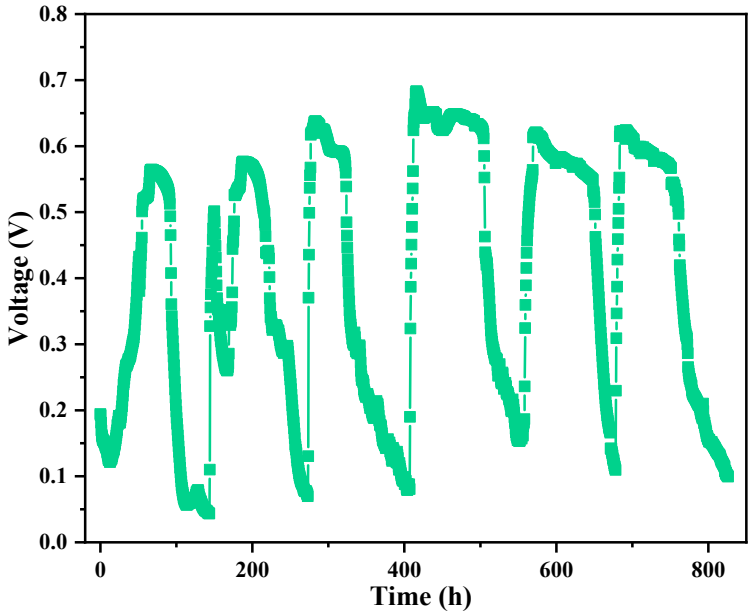

Fig. S3. The stable and repeatable voltage output generated by the anode of the enrichment stage MFC.

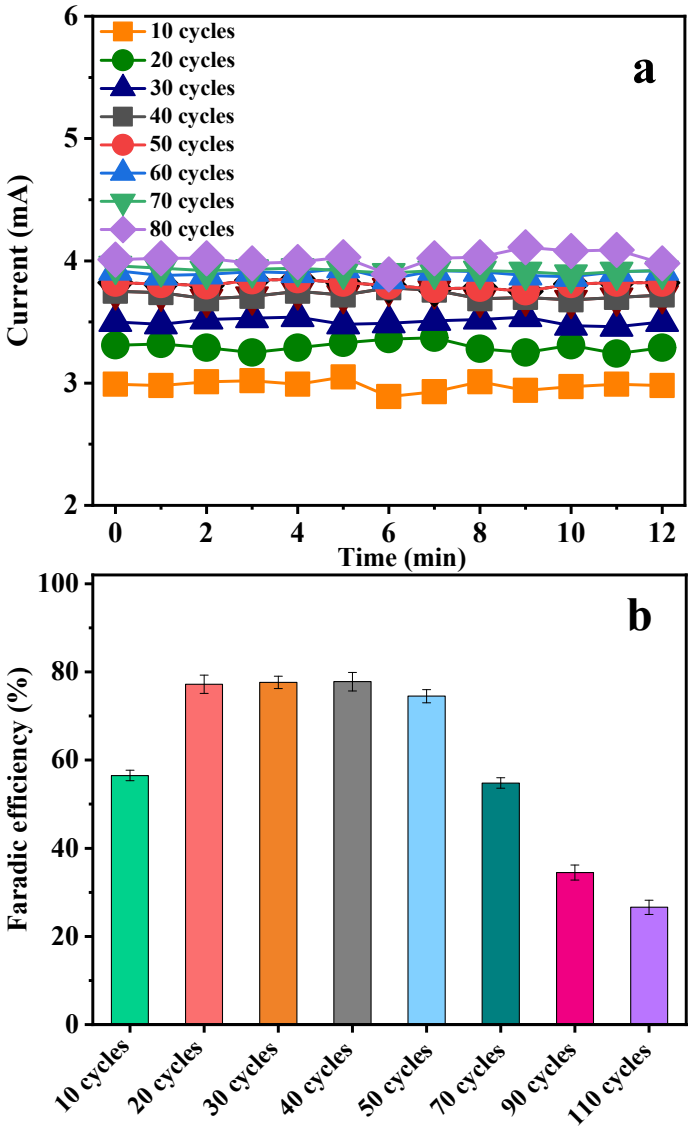

Fig. S4. The effect of pTTh catalyst layers thickness (current (a) and Fadaric efficiency (b)) on H_2O_2 production in the BSPS reactor.

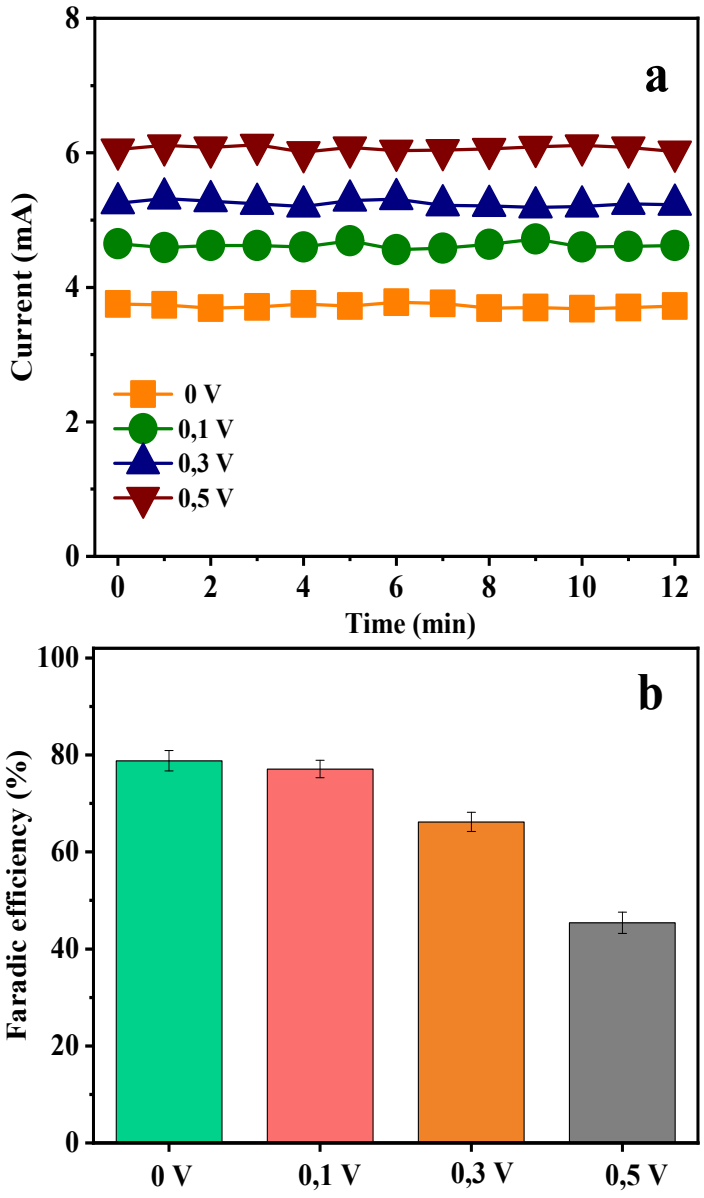

Fig. S5. The effect of applied voltage (current (a) and Faradic efficiency (b)) on H_2O_2 production in the BSPS reactor.

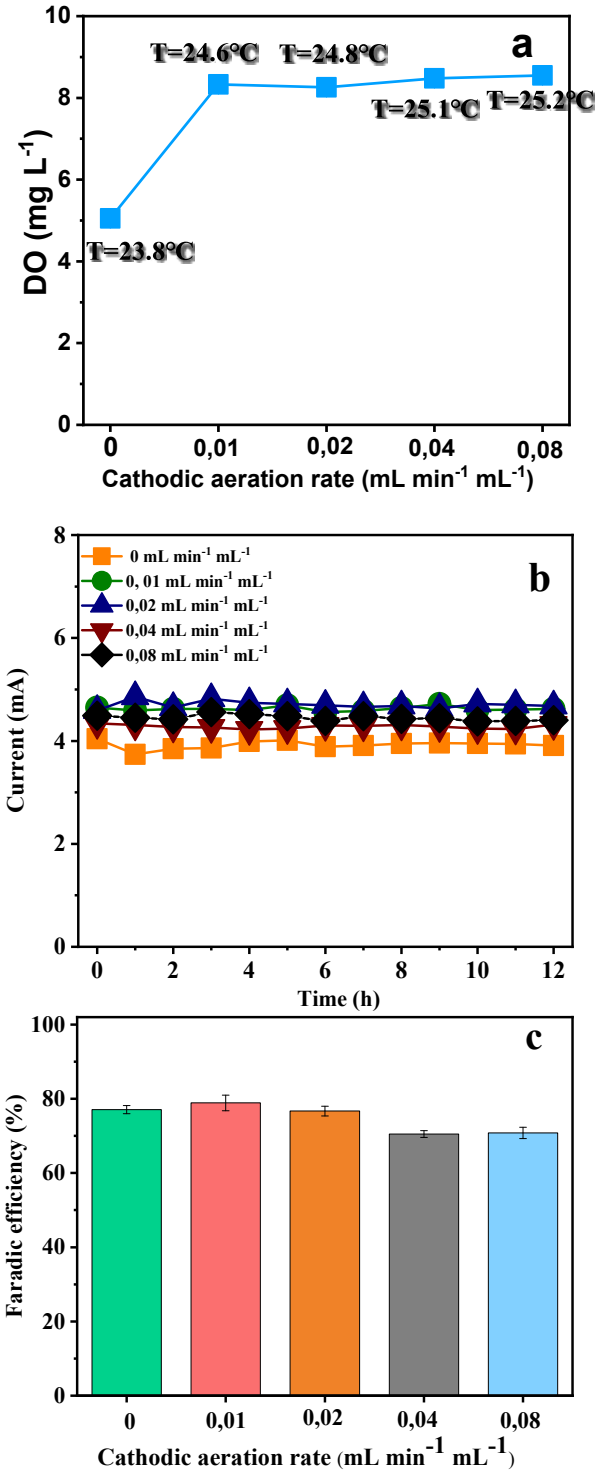

Fig. S6. The effect of cathodic areation rate (catholyte DO (a), current (b), and Faradic efficiency (c)) on H_2O_2 production in the BSPS reactor.

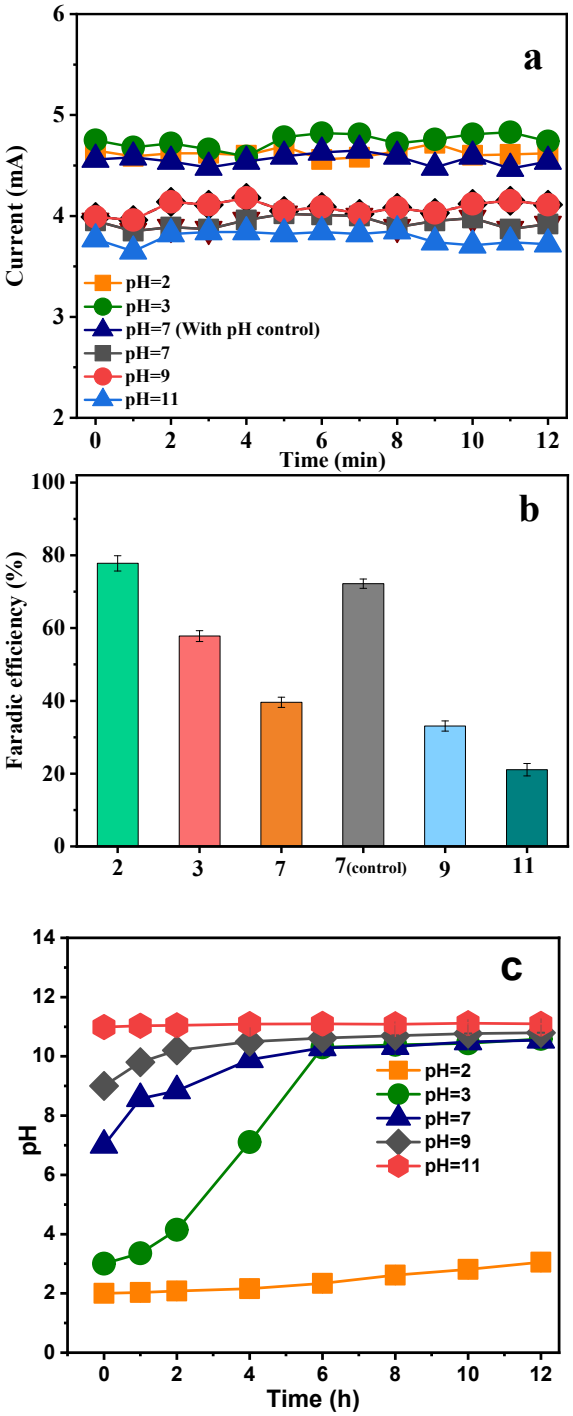

Fig. S7. The effect of initial catholyte pH (current (a), Faradic efficiency (b), and catholyte pH variation (c)) on H_2O_2 production in the BSPS reactor.

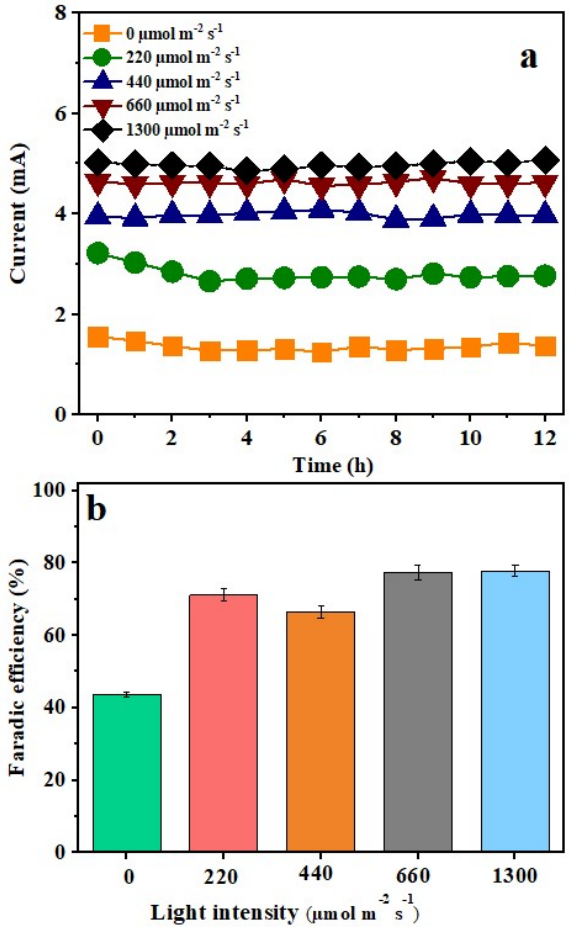

Fig. S8. The effect of light intensity (current (a) and Faradic efficiency (b)) on H_2O_2 production in the BSPS reactor.

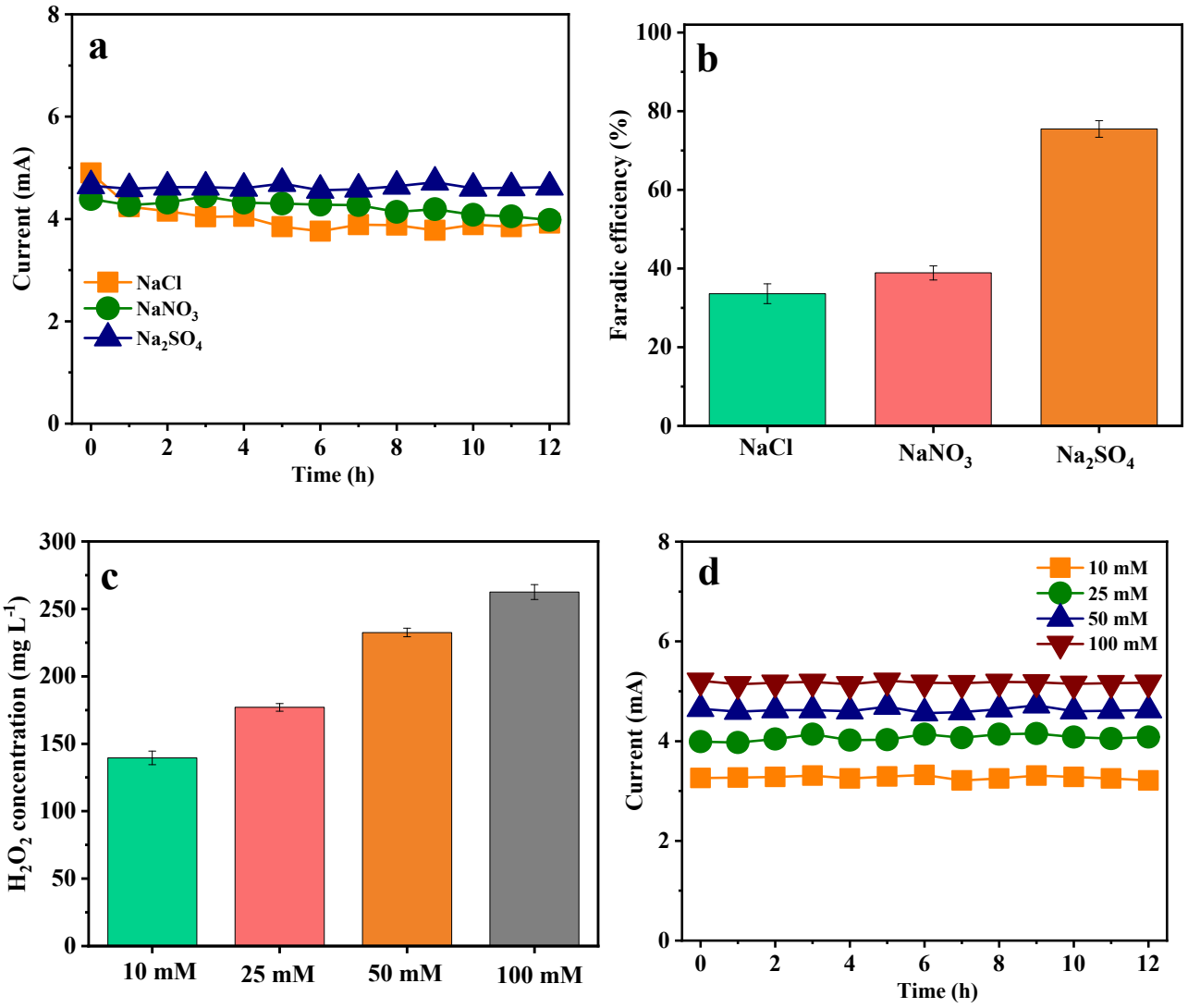

Fig. S9. The effect of electrolyte nature (current (a) and Faradic efficiency (b)) and concentration (accumulated H_2O_2 concentration (c) and current (d)) on H_2O_2 production in the BSPS reactor.

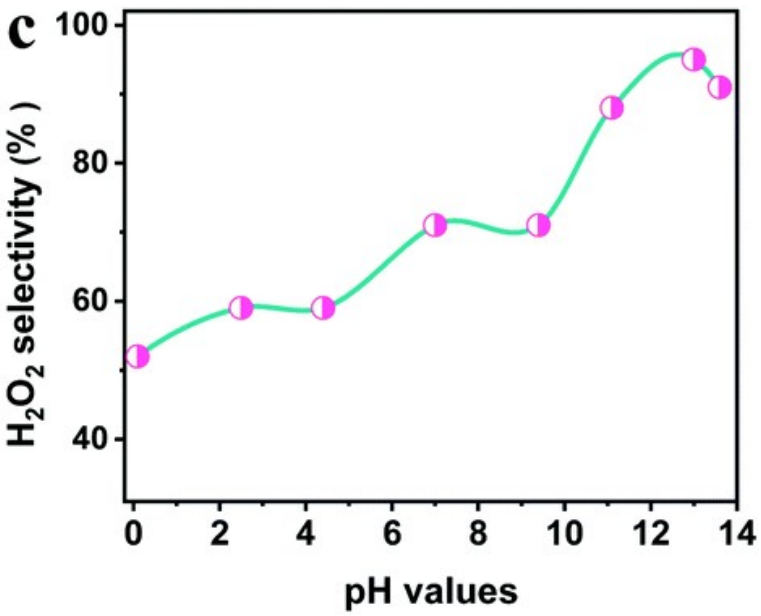

Fig. S10. pH dependent H_2O_2 selectivity of pTTh calculated by RRDE results [11].

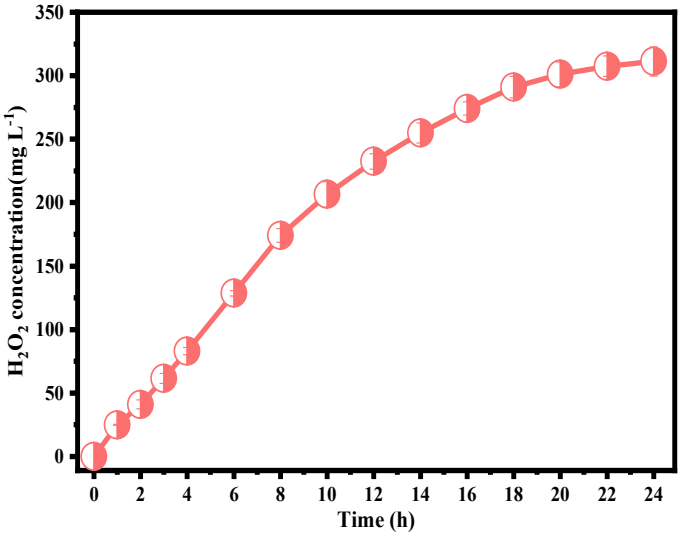

Fig. S11. Concentration of H_2O_2 produced cumulatively with reaction time in BSPS reactor.

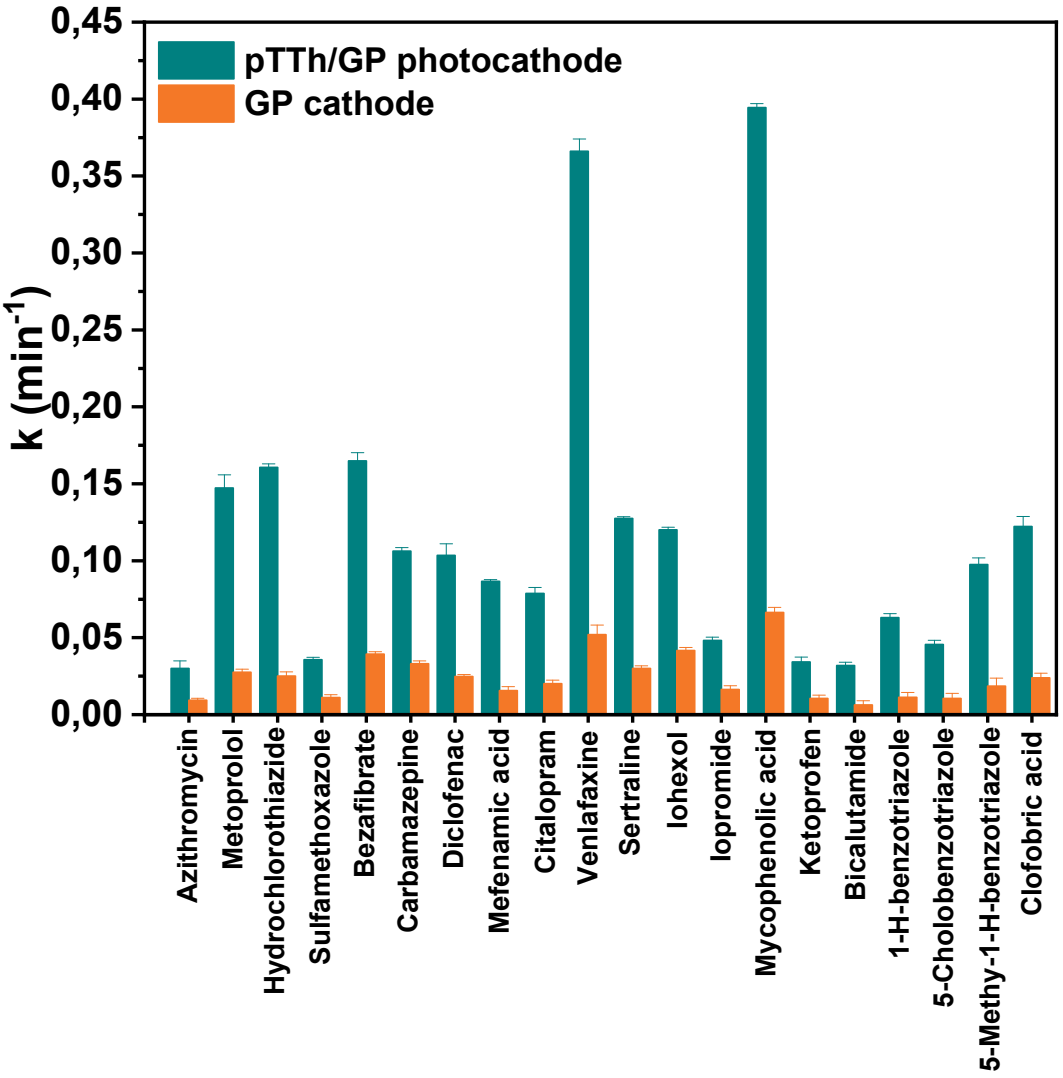

Fig. S12. Pseudo-first-order rate constants (k) of the degradation of 20 typical micropollutants from WWTP secondary effluent during BSEF treatment using pTTh/GP photocathode electrode and GP cathode, respectively.

References

1.Fu, L., You, S.J., Yang, F.l., Gao, M.m., Fang, X.h. and Zhang, G.q. Synthesis of hydrogen peroxide in microbial fuel cell. J. Chem. Technol. Biot. **2010,** 85(5), 715-719.

2. Li, N., Wang, S., An, J. and Feng, Y. Acid pretreatment of three-dimensional graphite cathodes enhances the hydrogen peroxide synthesis in bioelectrochemical systems. Sci. Total. Environ. **2018,** 630, 308-313.

3. Chen, J.-y., Li, N. and Zhao, L. Three-dimensional electrode microbial fuel cell for hydrogen peroxide synthesis coupled to wastewater treatment. J. Power Sources **2014**, 254, 316-322.

4. Chen, J.-y., Zhao, L., Li, N. and Liu, H. A microbial fuel cell with the three-dimensional electrode applied an external voltage for synthesis of hydrogen peroxide from organic matter. J. Power Sources **2015**, 287, 291-296.

5. Li, N., An, J., Zhou, L., Li, T., Li, J., Feng, C. and Wang, X. A novel carbon black graphite hybrid air-cathode for efficient hydrogen peroxide production in bioelectrochemical systems. J. Power Sources **2016,** 306, 495-502.

6. Young, M.N., Links, M.J., Popat, S.C., Rittmann, B.E. and Torres, C.I. Tailoring microbial electrochemical cells for production of hydrogen peroxide at high concentrations and efficiencies. ChemSusChem **2016,** 9(23), 3345-3352.

7. Modin, O. and Fukushi, K. Development and testing of bioelectrochemical reactors converting wastewater organics into hydrogen peroxide. Water Sci Technol. **2012,** 66(4), 831-836.

8. Sim, J., Reid, R., Hussain, A., An, J. and Lee, H.-S. Hydrogen peroxide production in a pilot-scale microbial electrolysis cell. Biotechnol. Rep. **2018,** 19, e00276.

9. Zou, R., Hasanzadeh, A., Khataee, A., Yang, X., Xu, M., Angelidaki, I. and Zhang, Y. Scaling-up of microbial electrosynthesis with multiple electrodes for in situ production of hydrogen peroxide. IScience **2021**, 24(2), 102094.

10. Zou, R., Rezaei, B., Keller, S.S. and Zhang, Y. Additive manufacturing-derived free-standing 3D pyrolytic carbon electrodes for sustainable microbial electrochemical production of H_2O_2. J. Hazard. Mater. **2024**,, 133681.

11. Fan, W., Zhang, B., Wang, X., Ma, W., Li, D., Wang, Z., Dupuis, M., Shi, J., Liao, S. and Li, C. Efficient hydrogen peroxide synthesis by metal-free polyterthiophene via photoelectrocatalytic dioxygen reduction. Energy Environ. Sci. **2020,** 13(1), 238-245.